Bonding and Magnetism in High Symmetry Nano-Sized Graphene Molecules: Linear Acenes C4m+2H2m+4 (m = 2,… 25); Zigzag Hexangulenes C6m**2H6m (m = 2,… 10); Crenelated Hexangulenes C6(3m**2-3m+1)H6(2m-1) (m = 2,… 6); Zigzag Triangulenes Cm**2+4m+1H6m (m = 2, … 15)

著者	Philpott Michael R., Cimpoesu Fanica, Kawazoe Yoshiyuki
journal or publication title	Materials Transactions
volume	49
number	11
page range	2448-2456
year	2008
URL	http://hdl.handle.net/10097/52172

Materials Transactions, Vol. 49, No. 11 (2008) pp. 2448 to 2456
Special Issue on Advances in Computational Materials Science and Engineering V

Bonding and Magnetism in High Symmetry Nano-Sized Graphene Molecules: Linear Acenes $C_{4m+2}H_{2m+4}$ ($m = 2, \ldots 25$); Zigzag Hexangulenes $C_{6m^{**}2}H_{6m}$ ($m = 2, \ldots 10$); Crenelated Hexangulenes $C_{6(3m^{**}2-3m+1)}H_{6(2m-1)}$ ($m = 2, \ldots 6$); Zigzag Triangulenes $C_{m^{**}2+4m+1}H_{6m}$ ($m = 2, \ldots 15$)

Michael R. Philpott[1,*], Fanica Cimpoesu[2] and Yoshiyuki Kawazoe[1]

[1]*Center for Computational Materials Science, Institute for Materials Research, Tohoku University, Sendai 980-8577, Japan*
[2]*Institute of Physical Chemistry, Splaiul Independentei 202, Bucharest 060021, Romania*

Plane wave based *ab initio* DTF all valence electron spin polarized calculations are reported for the electronic structure and geometry of differently shaped graphene molecules. These polycyclic hydrocarbon molecules comprise four series: D_{2h} symmetric linear polyacenes $C_{4m+2}H_{2m+4}$ ($m = 2, \ldots, 25$); D_{6h} hexagulenes with zigzag edges $C_{6m^{**}2}H_{6m}$ ($m = 2, \ldots, 10$); D_{6h} hexagulenes with crenelated edges $C_{6(3m^{**}2-3m+1)}H_{6(2m-1)}$ ($m = 2, \ldots, 6$); D_{3h} zigzag edged triangulenes $C_{m^{**}2+4m+1}H_{6m}$ ($m = 2, \ldots 15$). The systems variously display ground states that are spin paired singlet ($S = 0$), singlet anti-ferromagnetically ordered diradical and spin polarized $S = 1/2(m - 1)$. Molecules with zigzag edges show evidence of electron delocalization along the perimeters with some bond alternation at the corners. In the acenes the spin paired singlet state of the short members switches to a singlet diradical at $m \approx 7$–8 and this remains as the ground state for larger m. In contrast the triangulenes are magnetic and the atomic charge and spin density changes monotonically with distance from center to perimeter. In the hexagonal systems the development of a graphene core region, where the C-C bonds are 142 pm, extends to within a few C-C bonds of the perimeter atoms. Zigzag hexagulenes have a spin paired singlet ground state for $m \leq 8$ and a singlet diradical ground state for larger m. When hexagulenes are substitutionally doped with boron or nitrogen, acceptor or donor levels appear that track the valence or conduction band edges with increase in zigzag number. This result suggests the possibility of building several semiconductor device structures into the same graphene molecule. [doi:10.2320/matertrans.MB200822]

(Received May 2, 2008; Accepted June 18, 2008; Published August 20, 2008)

Keywords: *density functional theory (DFT), linear acene, triangulene, hexagulene, graphene, zigzag edge, crenelated edge, polycyclic hydrocarbon, fully benzenoidal hydrocarbon, diradical, spin density, boron doping, nitrogen doping, Kohn-Sham levels*

1. Introduction

First principles plane wave based DFT calculations are described that explore the electronic and geometric properties of a variety of differently shaped planar polycyclic hydrocarbon molecules with sizes up to 6 nm. We refer to these entities as graphene molecules since they are composed of condensed "aromatic" hexagonal shaped C_6 rings with one p_z-orbital electron for every carbon atom. They may be thought of as nano-sized fragments of graphene in which any edge carbon atom with an unsaturated valence is terminated with a hydrogen atom. Figure 1 displays all the systems examined in the present study. The aromatic rings of the crenelated (so called arm chair) edge graphenes are shown using the circle notation which is widely used to designate the location of the aromatic sextet rings of a fully benzenoidal hydrocarbon.[1,2)]

Scientific and technological interest in graphene as a material for electronics was sparked by the discovery that large micron sized sheets of graphite a few carbon atoms thick could be sloughed from a bulk crystal.[3,4)] This remarkable finding was followed by another discovery, that some sheets were one atom thick and so resembled an unrolled single walled carbon nanotube. Previous to this discovery, fullerene nanotubes were being widely studied as sub micron sized components for molecular-electronic devices.[5)] However a nano-electronics technology based on large planar graphene sheets has obvious practical advantages over tubes, the chief being that devices based on sheets could be developed with an evolution of existing planar silicon technology and instrumentation. Tube-technology on the other hand has significant issues of both conceptual and technological nature and would very likely require some revolutionary advances[6)] before any robust operational devices could be manufactured.

This recent stunning progress in graphene science and technology aside, our work is also motivated by other science old and new, including for example:

(1) The *tour-de-force* synthesis of the D_{6h} symmetric crenelated polyaromatic hydrocarbon $C_{222}H_{42}$ and related materials by K. Müllen and coworkers;[7,8)]
(2) the proposed singlet diradical ground state for linear polyacenes longer than heptacene;[9,10)]
(3) the historical record which documents, in the development of quantum chemistry starting from the 1930s,[11–13)] the important overlapping concepts of conjugated C-C double bonds and aromaticity in novel forms and guises[14)] in the polyenes, polycyclic hydrocarbons[15–19)] and annulenes.[20)]

This paper is organized as follows. Following this introduction we provide a sparse account of the computational method. Next in separate sections we describe the four categories of graphene hydrocarbon considered in this study: linear acenes with a discussion of the $S = 0$ diradical and spin states $S = 1$ and 2 states for $m > 7$; zigzag edged hexagulenes, with a discussion of edge state electron delocalization,

*Corresponding author, E-mail: philpott@imr.edu

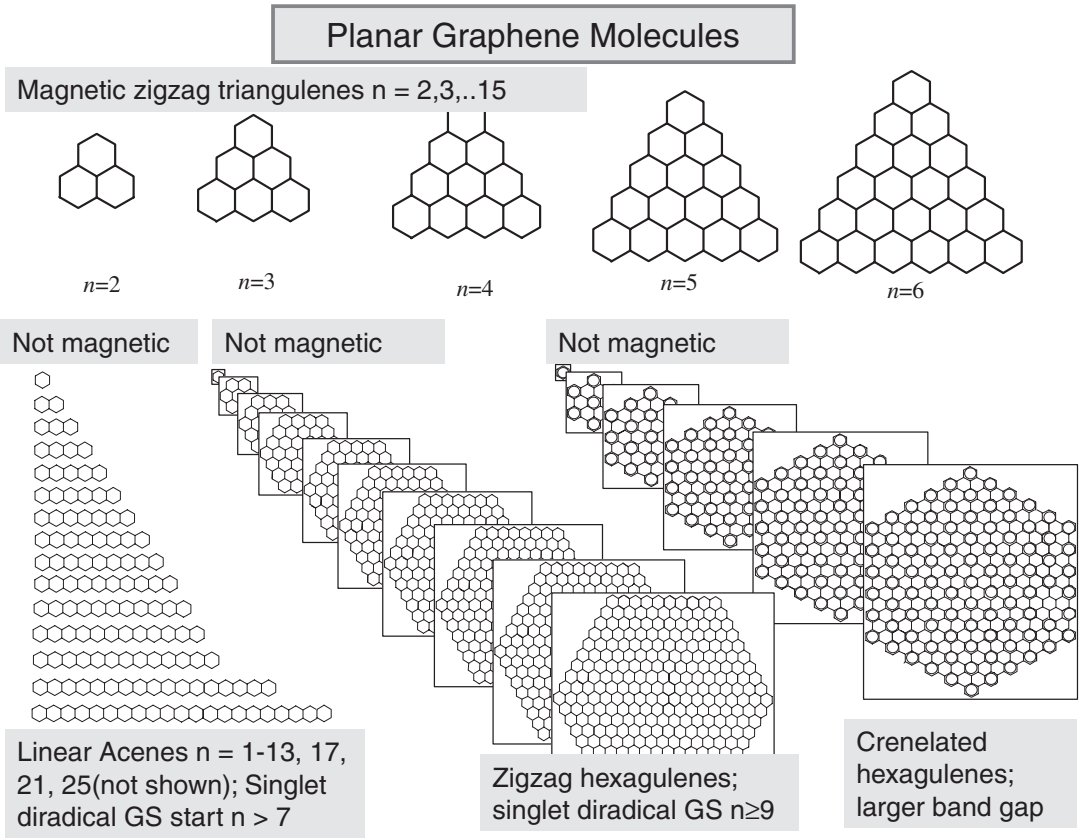

Fig. 1 Schematic diagram of four series of graphene molecules: linear D_{2h} acenes (left), zigzag D_{3h} triangulenes (top), zigzag D_{6h} symmetric graphenes (bottom center) and crenelated or arm chair D_{6h} graphenes (bottom right). The labels describe important properties of the series. For example, the linear acenes and both hexagulenes are not magnetic for small zigzag ring number n.

growth of the central graphene zone and appearance of a diradical singlet ground states for $m > 8$; crenelated (arm chair) edged graphenes with a discussion of the assumptions underlying their description in terms of the aromatic sextet applied to large fully benzenoid hydrocarbons; zigzag edged triangularenes with a discussion of the distribution of ferromagnetically aligned spin density in the ground state. This paper is concluded with a discussion of the energy levels of hexagulenes substitutionally doped with boron and nitrogen to produce molecules with thermally accessible hole and electron conducting states.

2. Computational Method and Diradical Reference Calculations

2.1 Methodology

In the calculations reported here we used *ab initio* plane wave based DFT calculations,[21–25] PAW frozen core pseudopotentials[26,27] and the spin polarized generalized gradient approximation for the exchange-correlation energy functional parameterized by Perdew and coworkers.[28,29] There are no basis set superposition errors (the basis set is huge) and the basis can be improved by increasing size of the simulation cell and the cut-off energy E_{cut} (acenes and hexagulenes 400 eV; triangulenes 500 eV) for the plane waves. Valence electrons were assigned: C (4) and H (1). All calculations were performed using periodic boundaries with tetragonal or orthorhombic periodic cell for which the a and b cell lengths were a minimum of 1.5 nm longer than either the long (L) and medium (M) in plane molecular geometry axes including the hydrogen atoms and a c unit cell length equal to 1.5 nm. This is much greater than the graphite interlayer spacing 0.167 nm. In this geometry there were no inter molecular atom-atom distances less than or equal to 1.5 nm. The Brillouin zone integration was restricted to the gamma point. The geometry optimizations were carried out using the conjugate gradient method until the forces acting on each atom were close to or less than 0.05 meV/pm. In this work we calculated geometry, total energy and isometric surfaces of total charge and spin density (where appropriate) for spin states $S = 0, 1, 2$ (occasionally). The calculations for the triangulenes were always performed with unrestricted spin and it was found that the total spin of the ground state invariably converged to $2S = (m - 1)$ unpaired spins. In most cases the starting geometries were constructed using standard CC and CH bond distances for aromatic hydrocarbons. The charge densities were analyzed using the vaspview program and the geometry was visualized using the free software Rasmol.[30]

2.2 Diradical benzene reference calculations

We have calculated the electronic structure, geometry and bonding in ground and first triplet state of the benzene molecule C_6H_6. This provides a measure of reassurance that the plane wave based single determinant wavefunction methodology used here can get close to results of other *ab initio* methods. For example, in the case of benzene

we obtained : Ground ($S = 0$) state: total energy $E = -76.234$ eV, homo-lumo energy gap $= 5.100$ eV; geometry C-C $= 139.65$ pm. In the first excited triplet ($S = 1$) diradical state of benzene ($\Delta E_{ST} \approx 4$ eV) there are two D_{2h} symmetric geometries with almost the same energy. Conformation S1a: total energy $E_{1a} = -72.262$ eV: geometry CC $= 151.6$ (2 long bonds), CC $= 138.9$ pm (4 short bonds). Conformation S1b: total energy $E_{1b} = -72.253$ eV; geometry CC $=$ 135.1 (2 short), CC $= 147.4$ pm (4 long). These conformations appear to be the same as two symmetric states calculated by the Israeli group[31] by a different method. The S1a triplet has two short parallel CC bonds with the spin localized on the para-located carbon atoms C1 (as in $CH^{\bullet}$) and C4 (again like $CH^{\bullet}$). The other S1b triplet state has a two long parallel *CC* bonds which separate the atoms C6-C1-C2 from C3-C4-C5. There is one spin delocalized over each of these groups which resemble a conjugated $C_3H_3^{\bullet}$. The calculations are consistent with the idea that the lowest triplet state of benzene molecule is "anti-aromatic", since the count of spin paired π-electrons is smaller by two, and as in the much studied molecule cyclobutadiene C_4H_4 the lowest excited triplet state of benzene can distort into two geometrically separate configurations.[32]

3. Linear Acenes-Zigzag Edges with No Graphene Interior

In the development of quantum theory of chemical bonds the properties of polyacene molecules $C_{4m+2}H_{2m+4}$ ($m = 1, 2, 3, \ldots$) were of interest because experiments and theoretical studies showed that the resonance stabilization energy, which is very high in benzene ($m = 1$), decreased rapidly with increase in the number of rings m.[15–20] The earliest semi-empirical calculations indicated that the band gap would decrease to zero near $m = 10$. In more modern times studies based on physically appealing model Hamiltonians, predicted that long or infinite acenes could exhibit phenomena such as conductivity, magnetism and even superconductivity.[33] Several calculations predicted that around $m = 7$–8 (heptacene-octacene) the homo-lumo single particle gap and the lowest singlet-lowest triplet state energy difference, approach zero. At this point a Peierls-like distortion[34] of the geometry could open a gap in the energy spectrum and new physical regime entered. Houk, Bendikov and coworkers,[9,10] on the basis of extensive *ab initio* calculations, were the first to predict that in the linear acenes a magnetic phenomenon occurred and the ground electronic state would become a disjoint singlet diradical.[35] In this state the spin "up" and spin "down" electrons occupy different sites with an anti-ferromagnetic pattern. There have been other recent studies of this effect,[36–40] some overlapping the time frame of this present study. The existence of a singlet or a higher spin ground state (radical) phase in the long acenes is connected to the influence of geometry of the perimeter on bipartite lattices. One important issue is how perimeter shape dependence can affect the transport of spin polarized charge in graphene devices.

In this section we report on several aspects concerning the lowest energy levels of the linear acenes, $C_{4m+2}H_{2m+4}$ ($m = 2, \ldots, 12, 13, 15, 17, 19, 21, 25$). The focus is on $S = 0$ spin paired, $S = 0$ diradical and $S = 1$ triplet states. Figure 2 shows the variation along the series $m = 3, \ldots, 25$ of the singlet band gap (BGS0 and BGS00), singlet-first triplet ($S = 1$) splitting (ES1-ES0 and ES1-ES00), singlet-quadruplet ($S = 2$) splitting (ES2-ES00), singlet spin paired and singlet diradical state (ES0-ES00). All energies (ordinate) are in eV. The labels beginning with "B" denote the difference between Kohn-Sham levels, so that BGS0 signifies the homo-lumo gap (D_{2h} symmetry) in the spin paired singlet range $m \leq 8$, and BGS00 is the homo-lumo gap (C_{2v} symmetry) for $m \geq 8$. The labels beginning with "E" denote an energy difference between states, so that ES0-ES00 is the energy difference between singlet spin paired (D_{2h} geometry) and singlet diradical (C_{2v} geometry, discussed below). Note that all the curves begin or end at zigzag (ring) number $m = 8$, the point where the ground state is a singlet diradical; data points for benzene ($m = 1$) and naphthalene ($m = 2$) are omitted from Fig. 2.

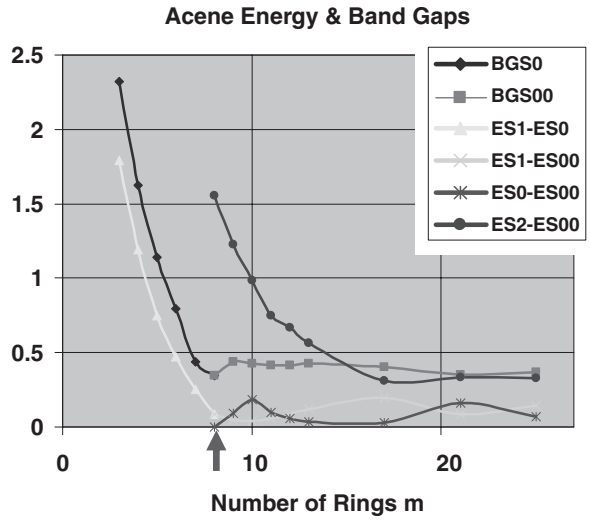

Fig. 2 Energy level differences and spin state energy gaps (eV) of the linear acenes plotted versus ring number $m = 3, \ldots 25$. All curves end or begin at $m = 8$ (arrow on the coordinate axis), the point where the ground state switches from singlet spin paired to singlet diradical. Curve labels: Kohn-Sham homo-lumo energy difference (BGS0, –◆–) for $m \leq 8$ and (BGS00, –■–) for $m \geq 8$; singlet-triplet energy gap (ES1-ES0, –▲–) for $m \leq 8$ and (ES1-ES00, –×–) for $m \geq 8$; singlet spin paired–singlet diradical energy gap (ES0-ES00, –∗–) for $m \geq 8$; singlet-quintruplet energy gap (ES2-ES00, -●-) for $m \geq 8$.

The $S = 0$ spin paired and $S = 0$ diradical state have essentially the same energy near $m = 7$ (heptacene), for $m > 7$ the diradical configuration becomes the ground state with C_{2v}(M) symmetry and is described more fully below. The $S = 2$ quadruplet was calculated for the long acenes because it does not correspond a real state of short acenes. Note that the curve BGS0 and its continuation BGS00 beyond $m = 8$ (marked by arrow on the coordinate axis) is the homo-lumo energy level difference from the system ground state, whereas the other curves are the difference between calculated system states. For large m (>15) the $S = 2$ configuration has approximately twice the energy of the $S = 1$ configuration which is consistent with the notion that both are delocalized over the molecule and to create an $S = 2$ state from $S = 1$ in a large system requires the addition of an energy quantum equal to that for the $S = 1$ transition. The

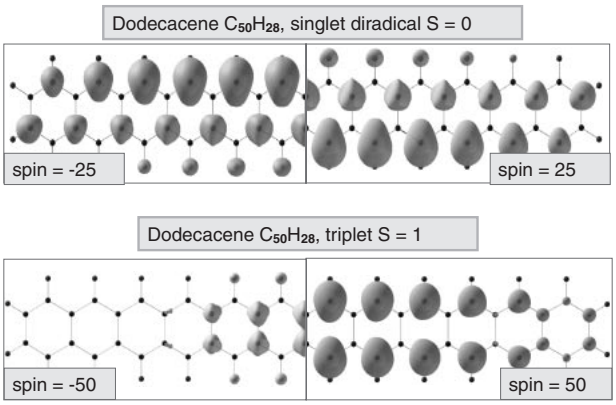

Fig. 3 Spin density in the linear acene ($m = 12$) dodecacene $C_{50}H_{28}$. Top panel, singlet ($S = 0$) diradical spin density isometric surfaces for spin values $d_{iso} = -25$ (LHS) and $+25$ (RHS). The complete densities are obtained by reflection left-to-right etc. Note the disjoint character of this state, spin up (+) and spin down (−) are confined to separate sub-lattices of the bipartite (alternate C atoms) carbon skeleton. Lower panel, diradical triplet ($S = 1$) state spin densities for spin values $d_{iso} = -50$ (LHS) and $+50$. Spin density is concentrated in spin up (+) configuration and there is the same signed spin on all last ring carbon atoms in the RHS sub-panel.

energy of the D_{2h} triplet $S = 1$ state becomes very close to the D_{2h} singlet $S = 0$ energy at $m = 7$ and in symmetry constrained geometry optimizations can even drop below it for $m \geq 8$.

Our new work extends previous work to very long acenes. For dodecacene we have explored numerous symmetries to find which geometric distortion promotes the formation of the diradical state. To this end we constrained the dynamics used in the geometry optimization to have the symmetry D_{2h}, C_{2h}(N), C_{2v}(L), C_{2v}(M), C_{2v}(N) and D_2. We found that the lower energy diradical state occurred using C_{2v}(M) geometry optimization, while most others reverted to the energy of the D_{2h} state. In the longest systems ($n \geq 12$) we found: diradical singlet $S = 0$ to be approximately 0.06 eV below the D_{2h} singlet $S = 0$; D_{2h} triplet ($S = 1$) and D_{2h} quintuplet ($S = 2$) state higher than the diradical ground state by approximately 0.09 eV and 0.67 eV respectively.

Figure 3 shows selected isometric surfaces of the spin density of the molecule dodecacene for spin 1 (+, up) and spin 2 (−, down) in the singlet diradical ground state and the lowest triplet state. Top panel Fig. 3 shows the diradical ground state. The left side shows the isometric surface for spin $d_{iso} = -25$ and the right side the spin distribution at $d_{iso} = 25$. The range of spin values in arbitrary units is $(-2157, 2144)$ and corresponds to maximum spin density of about 0.2 spins/Å^3. The spin distribution is characteristic of a disjoint radical,[35] the sign is unique to the bipartite sub-lattice. The spin density from LHS to RHS switches from one alternant lattice to the other. The highest spin density regardless of spin axis direction is on C atoms with an H atom attached. The two highest homos carry the spins of opposite sign in disjoint diradicals.[35] The lower panel of Fig. 3 shows the isometric surfaces of spin distribution in the lowest triplet state.

The spin pattern is different, the highest (+)-spin is on C atoms with attached H regardless of sub lattice and there is much less spin on the negative spin isometric surface. Another difference is an end effect in the end rings which have the same signed spin on all six atoms. The range of spin values in arbitrary units is $(-360, 2155)$ and corresponds to a maximum spin density of about 0.2 spins/Å^3.

In linear acenes $m \geq 8$ the cross bonds in the middle of the molecule joining opposing edges have CC $\approx$ 145 pm. This suggests that stretching the cross C-C bonds in short linear acenes could force the molecule into a diradical state. We have checked this idea with calculations on benzene, naphthalene and anthracene in which we biased the starting spin-geometry configuration with an anti-ferromagnetic spin distribution. For acenes with $m = 1, 2, 3$ parallel pair(s) of cross C-C bonds were stretched to approximately 240 pm. In this geometry the calculations showed diradicals ($S = 0$ and $S = 1$) with spin patterns similar to the long acenes.

In the diradical electronic ground state the pattern of CC bond lengths along the edge provides information on electron delocalization along the chain. At each end of the molecule there is a cis-butadiene bond pattern (short-long-short) that joins the two opposing parallel chains. The butadiene "double" bond, length CC $\approx$ 136 pm, pins one end of a sequence of alternating bonds. Going towards the centre of the chain, the alternation weakens and the C-C bonds become more uniform. Simultaneously the cross CC bonds increase from CC $\approx$ 142–143 pm at the butadiene end to CC $\approx$ 145–146 pm near in the center of a chain in a molecule like dodecacene. All the long acene molecules are wider in the middle than at the ends. This geometry is consistent with the notion of increased electron delocalization along the chain in the middle with reduced cross CC bonding. Imprinted on this pattern there are others in DFT modelling. For example, we have noted small non monotonic structural variations that could arise from incommensurability of the delocalized electron and/or the constraints imposed on the chain by the cross bonding.

4. Hexagulenes with Zigzag Edges and D_{6h} Symmetry

Pioneering early work on large hexagulene molecules was described by Stein and Brown.[41] Using Hückel, extended Hückel theory and structure resonance theory they examined systems with several thousand atoms. This was an important contribution. Since then many papers have appeared describing the band structure and possible magnetism of graphene strips at various levels of approximation. To our knowledge only two groups have considered aspects of hexagonal systems[42,43] in a general way. None have studied the geometry or the electronic structure at the level of detail provided here. Hexagulene with eight rings on edge was predicted to be an anti-ferromagnet.[42] The calculations described here predict $n = 9$ as the first candidate.

Next we consider the electronic properties and geometric structure of planar D_{6h} symmetric graphene molecules with zigzag edges. The largest molecule is 5 nm in diameter (10 rings along each edge) and contains 660 atoms approximated by a total of 2460 valence electrons. Figure 4 shows the homo-lumo level gap (upper curve ■ data points) and the energy difference ΔE_{ST} (lower curve ◆ data points) between the spin paired singlet $S = 0$ ground state and the lowest $S = 1$ triplet state state for the zigzag and crenellated

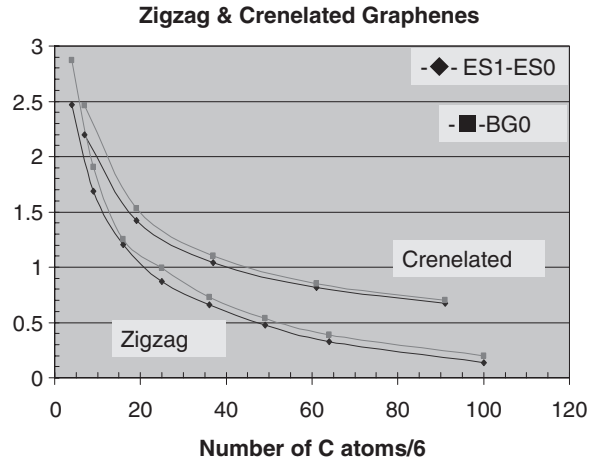

Fig. 4 Hexangulene electronic energy gaps (eV) vs. size (number of carbon atoms)/6 for the zigzag and crenelated series. Singlet homo-lumo energy level differences (BG0, –■–) eV and singlet-triplet (ES1-ES0, –◆–) energy gaps (eV). Zigzag series lower pair of curves and crenelated series upper pair of curves.

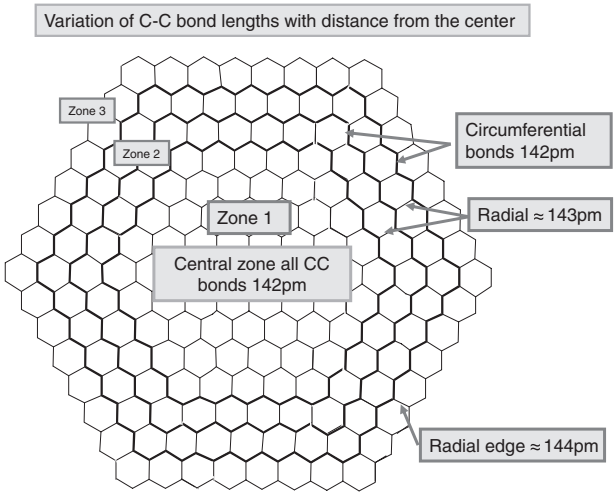

Fig. 5 Schematic diagram showing approximately the zones inside a D_{6h} symmetric 8-zigzag edge hexangulene molecule where the CC bonds have different lengths.

hexagulenes. The index "m" in the stoichiometric formula is not such a useful parameter for the coordinate axis, so instead we have used the number of C atoms in a molecule divided by six. This is equivalent to the number of benzenoid rings in the crenelated molecules.

Figure 4 shows that for both series the triplet-singlet energy difference ΔE_{ST} is smaller than the homo-lumo gap BG0. For benzene there is about one eV energy difference between BG0 and ΔE_{ST}. This difference erodes quickly with increasing size. Figure 4 also shows in the zigzag series the humo-lumo gap decreased faster with size compared to the crenellated series. We return to this topic again in the section describing the crenelated hexagulenes.

Figure 5, based on data from 8 zigzag hexagulene, shows a feature of all compact graphenes, namely the presence of an interior zone in which all bonds and angles approximate graphite plane values. The uniformity of central properties was assessed using isometric surfaces of the total and partial

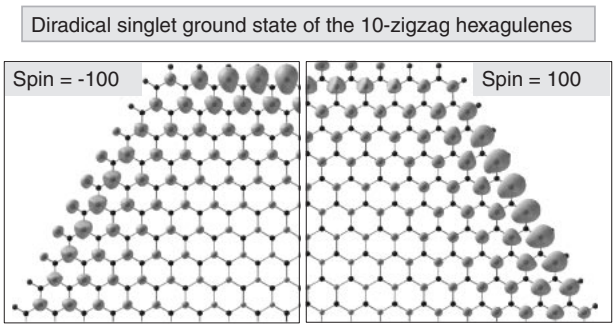

Fig. 6 Spin 1 (up, +) and spin 2 (down, −) density isometric surfaces for a quadrant of the diradical ground state of 10-zigzag hexagulene. Reflection in the (vertical) dividing line gives second quadrant. Note that in this disjoint diradical the carbon atoms carrying spin 1 (+) and spin 2 (−) are on different sub lattices of the bipartite lattice.

charge density, atomic electron density and bond lengths. There are several zones:

- An interior zone 1 where all the carbon-carbon bonds satisfy CC = 142 pm;
- A region two rings wide (zone 2) where the circumferential bonds are CC = 142 pm and the radial bonds are CC = 143 pm;
- Zone 3, the outer hexagonal ring of forty-two C_6 rings where the outer perimeter has CC bond alternation starting at the apex and fading to an almost uniform CC bond distance in the middle of the edge; and on the inside circumference the tangential CC = 142 and the radial CC = 144 pm.

The outer perimeter has features similar to the edges of the linear acenes. In the case of this 8-hexagulene the bond alternation pattern along an edge starting and ending at the apex was CC = 136-144-138-142-140-142-140-141-141-140-142-140-142-138-144-136 pm. The two apex atoms with attached H have the shortest bonds in the entire molecule C(H)-C(H) = 136 pm. This is expected to be the most reactive bond for substitution and addition reactions. The alternation of bond distances can be related to properties of the total electron charge density. The pattern of isometric surfaces of total charge density (combined densities of σ- and π-electrons) developed distinctive patterns with approximate double bonds at the apexes and CC bonds with alternating length extending from apex to the middle of the edge. This pattern resembles the acene pattern. The degree of bond alternation diminishes going towards the center of each edge corresponding to increased electron delocalization in the middle of the chain.

In this study a new phenomena appears at $m = 9$ for the zigzag hexangulenes. The ground state becomes a singlet diradical. This phenomenon has similarities to the linear acenes in the range $m = 7$–8. The DST calculations for $m = 9$, 10 showed the ground state to be a singlet diradical with D_{3h} symmetry. Figure 6 shows two isometric surfaces of spin density on quadrants of the largest molecule studied 10-hexagulene $C_{600}H_{60}$. There are similarities to the singlet ($S = 0$) diradical ground state of the long acenes. The spin density from LHS to RHS switches from one lattice to the other. The left side shows the isometric surface for spin $d_{iso} = -100$ and the right side the spin distribution at

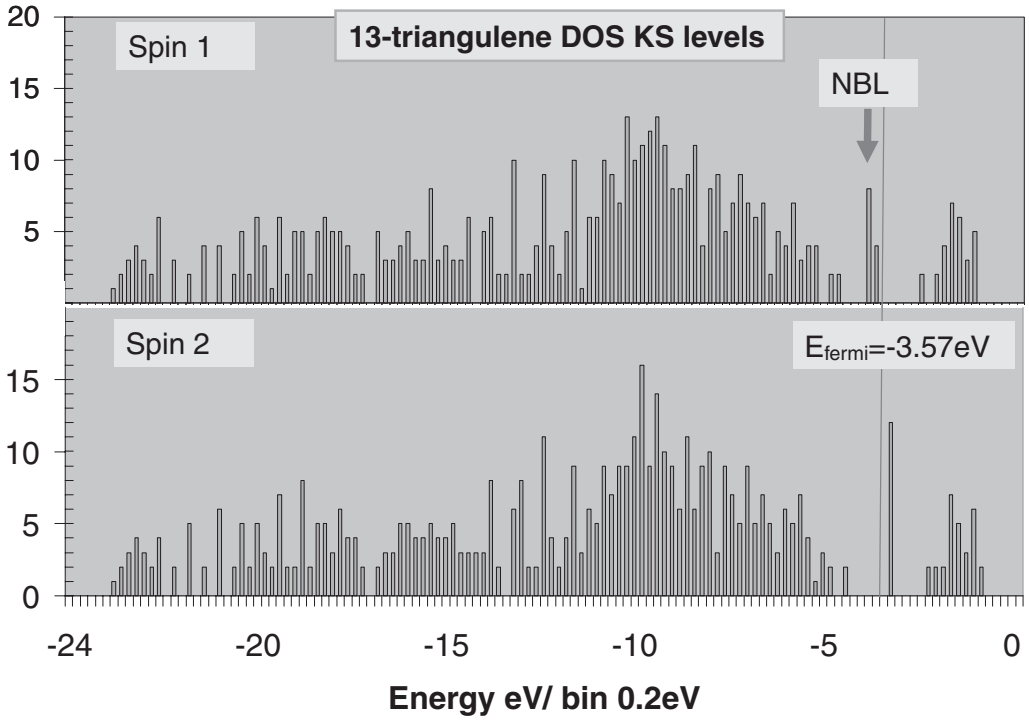

Fig. 7 Density of spin polarized Kohn-Sham levels in 13 zigzag triangulene plotted as a histogram with ordinate frequency in a 0.2 eV wide bin and coordinate bin energy (eV). Top panel, spin 1 (+) shows twelve occupied non bonding π-levels, the bottom panel spin 2 (−) shows the twelve unoccupied lumo levels just above the Fermi energy.

$d_{\rm iso} = 100$. The range of spin values in arbitrary units is $(-14469, 14469)$ which is equivalent to maximum spin density of 0.25 spins/Å^3. The spin distribution is characteristic of a disjoint radical[35] and the sign is unique to the bipartite sub-lattice. The highest spin density is associated with the edge and penultimate row C atoms. The spin density alternates in sign going around the edges in a sequential fashion. This pattern does not resemble that seen for the triplet $S = 1$ state which generally lies higher by 0.01–0.02 eV over the diradical ground state.

5. Comments on Hexagulenes with Crenelated Edges

Space does not permit an extended description of the crenellated series. The density of states of the largest zigzag and crenellated hexagulenes systems was found to be very similar except at the homo-lumo gap, implying that the central zone of both series is graphene-like. We consider the electronic charge density on the crenellated edge. The apexes of the crenellated series have five protruding carbon atoms (three with attached H atoms) that resemble the apexes lying on the L-axis of the PAH pyrene $C_{16}H_{10}$. The four carbon atoms comprising the crenelation on the edges resemble the total charge structure observed for the M-axis apexes of pyrene. In neither case do the carbon atoms of these C_6 rings have the uniformity of benzene. This distinction could be made more quantitative using the electron localization function[44,45] and the atoms in molecules theory.[46] For this discussion another observation is important, when we examine isosurfaces of the total charge distribution we find that the apex charge of the non-benzenoidal hydrocarbon pyrene resembles the perimeter charge of the crenelated fully benzenoidal hydrocarbon. The Clar hypothesis is based in part on the assumption that the two Kekulé valence bond resonance structures are responsible for the aromatic stabilization of the ring. From many perspectives this is known to be false. The early discussions of valence bond calculations concerning the stability of the benzene ring by Craig and others[47,48] noted that it was important to include not just neutral Kekulé, Dewar and prismane resonance structures but also a very large number of ionic structures. Modern work[49,50] has shown explicitly that in short acenes the Kekule structures contribute only 40%. As molecules get larger the number of ionic terms rises faster that the Kekulé ones so that in fully benezenoidal hydrocarbons the sextet stability contribution is swamped by the "ocean" of ionic ones. The edge in 2D presents an example of the classic problem in the coexistence of surface and bulk levels.

6. Triangulenes with Zigzag Edges and D_{3h} Symmetry

Next we report on calculations for the triangulenes with $m = 2, \ldots, 15$ zigzag edges. The two sub-lattices must now be distinguished (A sub-lattice has carbon atoms with attached H atoms at the edges; B sub-lattice has hydrogen atoms on apex carbon atoms). They have different numbers of carbon atoms, which permits a ferromagnetic arrangement of spins across the entire molecule[41,42] and a resulting net spin $S = 1/2(m-1)$. Figure 7 shows the calculated density of states (DOS) for separate spin polarized levels for the 13-zigzag triangulene. This DOS is a histogram of frequency of occurrence of Kohn-Sham energy levels (ordinate) against their energy (coordinate). The bin widths are 0.2 eV. The magnetism arises from twelve occupied non-bonding homo

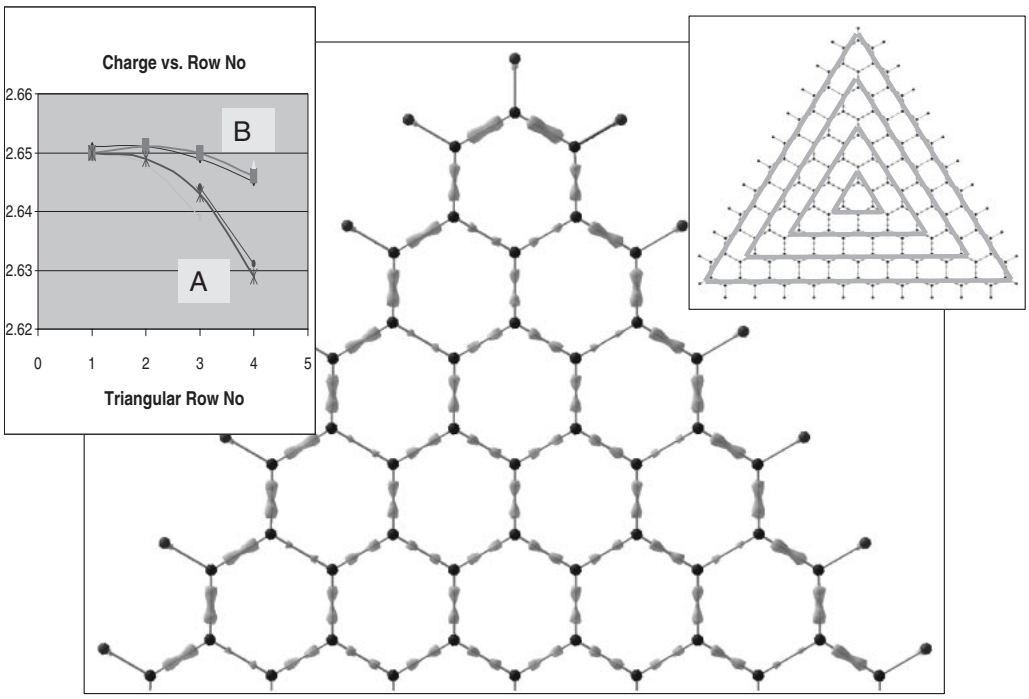

Fig. 8 An isometric surface for the total charge density of the molecule 10-zigzag triangulene. On this isometric surface the CC bonds around the perimeter all have a larger charge surface than in the interior. The apex carbon atom with attached H atom belongs to the B-sub lattice. The edge atoms are linked to the interior by "weaker" CC bonds with smaller sized isometric surfaces. Right inset, pattern of triangular rows 1(centre),... 4(edge). Inset left panel shows the variation of atomic charge by row for the A- and B-sub lattices. The spread in values arises because there are atoms in different local environments on the same row.

levels (NBL) bunched below the Fermi level and separated by approximately 1 eV from the π-bonding valence levels. Above the Fermi level there is a set of non-bonding lumo levels which are the counter parts of the occupied NBLs. The gap between these to two manifolds decreases smoothly with edge length.

The intra-spin band gap, approximately 1 eV, is the same for each separate spin manifold while the inter-spin band gap (for $m = 15$ triangulene) is approximately $\approx$0.3 eV. There is no evidence where in the series examined so far that a reduced band gap and or geometry change would depolarize the total spin for larger m values, leading to a reduced magnetic moment. Around the perimeter all the CC bonds $\approx$141 pm, while bonds pointing inwards from the perimeter have C-C bonds $\approx$144 pm. None of these latter C atoms have attached H atoms, the distinguishing difference between the spin up lattice (majority spin have attached H atoms on the edge) and spin down (minority spin).

Figure 8 shows a detail of an isometric surface of the total electronic charge for the 10-zigzag triangulene. Inset (RHS) is a schematic showing how carbon atoms can be assigned to triangular rings inside the molecule. Inset (LHS) is a plot of atomic charge as a function of the triangular row label 1, 2, 3, 4. The charge on the atoms decreases monotonically with distance from the center. There are two main groupings corresponding to major A (bottom group) and minor B lattices (top grouping). Within a group, the different lines arise from different environments on a given row. The greatest differentiation occurs for the A-sub lattice perimeter atoms because of the wide range of CC bond lengths. This figure shows the main physics is the change in environment of the two lattices with distance from the center and not between atoms belong to the same row. The geometry at the edges is quite different to the interior region. The apex carbon atoms have an electronic structure (revealed by isometric surface plots of the total charge density) that is distinctly different from the acenes and hexacenes. This is a result of overall D_{3h} symmetry and local site symmetry C_{2v} with an axis through the middle apical C atom. The topology of isometric surfaces of the total charge density of the three corner carbon atoms was found to resemble that around the apical C atom in pyrene.

Figure 9 shows the distribution of spin density for two oppositely signed isomeric spin density surfaces. Spin 1 (up) is only on the A-lattice and spin 2 (down) on the B-lattice. There is spin density on all the C atoms regardless of location in the interior or on the edges. In the interior the spin density is small, growing in magnitude by triangular row. The inset in Fig. 9 shows the variation of spin on atoms for the two lattices. The A-sub lattice, which has positive spin, shows the largest change with row number. The spins for different atoms belonging to the same row are bunched together. The environmental effects on spin show much more strongly than for the charge shown in Fig. 8.

7. Discussion/Summary

This report has touched on similarities amongst major categories of graphene molecule. Shape has a deciding effect on net magnetism and size on whether the ground state electric charge under goes spin polarization. Detailed work remains to be recorded to complete the account of the

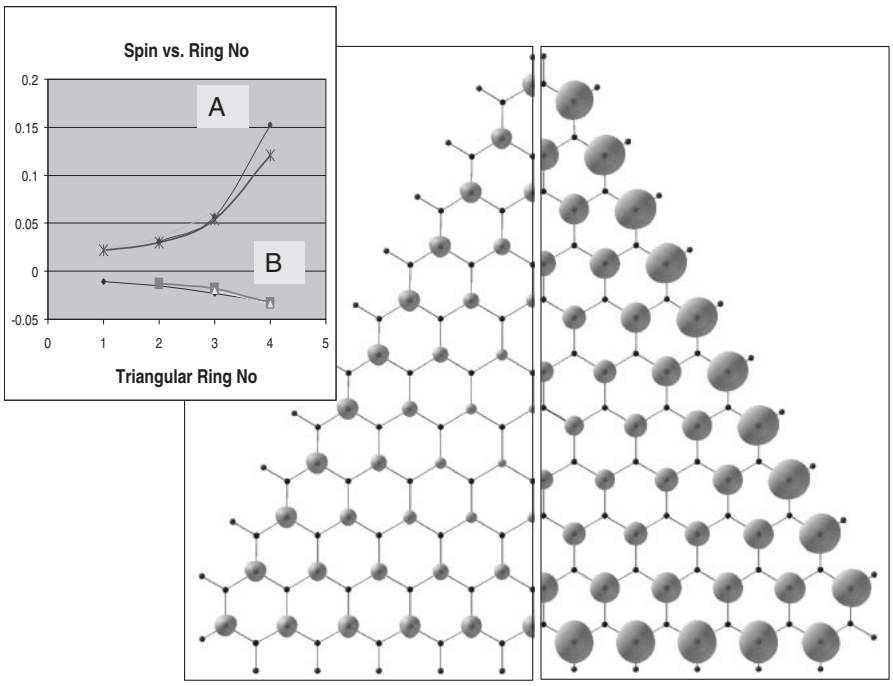

Fig. 9 Isometric surfaces for the total spin density for spin 1 (+, RHS) and spin 2 (−, LHS). The spin distribution is disjoint. Inset panel shows how the atomic spin on the different sub-lattices varies with the triangular rows depicted in Fig. 8. The spread in values arises from different atomic environments within a given row.

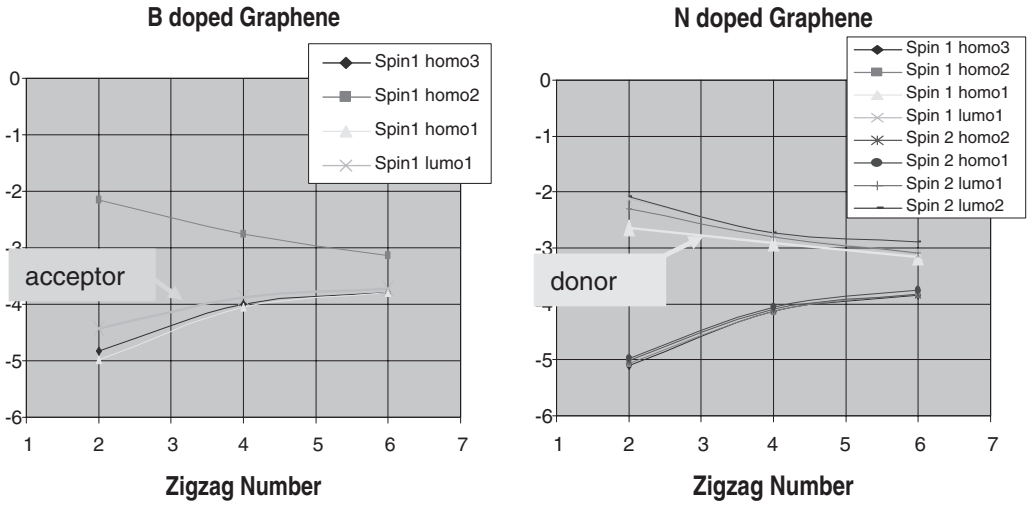

Fig. 10 Spin polarized Kohn-Sham homo and lumo energy levels of the zigzag hexagulenes $m = 2, \ldots, 6$ doped with a single atom of boron or nitrogen. The LHS panel shows the results of boron doping; only the spin 1 polarized Kohn-Sham levels are plotted. The lowest single electron lumo (spin 1 lumo-1, –×–) due to boron tracks the top of the valence band. The RHS panel shows the results for doping with nitrogen. In this RHS panel we have plotted the spin 1 and spin 2 Kohn-Sham levels. The single electron occupied homo (spin1 homo-1, –▲–) donor nitrogen level tracks the bottom of the conduction band.

calculations reviewed here. There is new work to report on the properties of excited electronic states, phonon-electron coupling and the splitting among NBLs in the triangulenes. We are also reminded that the graphene-like boride lattice in solid MgB_2 exhibits a superconducting phase transition at 60 K[51] so understanding the intricacies of phonon coupling in various geometries appears to be an interesting avenue for research. Graphite is well known for its ability to accept a variety of chemically different intercalants and some aspects of transition metal sandwiches with graphene molecules have studied.[52]

Finally as an application of the above ideas we describe the effect of single atom doping on the zigzag hexagulene systems. Substitutionally replacement (doping) of just one centrally located C atom in the zigzag series of the hexagulenes with B or N atoms produces molecules which when linked to electrodes could respond with hole and electron semiconductor properties. Figure 10 shows results from spin polarized DFT calculations for these odd electron systems. The ordinate is the energy (eV) of four Kohn-Sham homo-lumo levels as a function of increasing molecular size measured by the zigzag number m. In the N doped system for

spin 1 (+ spin) there are three homos and one lumo, and for spin 2 (− spin) there are two homos and lumos in the band gap region. The highest homo tracks and approaches the lumo level so that at $m = 6$ they are close together even though the band gap of the undoped molecule is still large. In the B doped system we show for spin 1 the two homos and two lumos. Now the lowest lumo tracks the valence band edge so that at finite temperatures promotion from the valence edge states would induce a hole in the valence manifold. In these systems the conductivity would depend on the relative positions of dopants and the distance to the perimeter. This, as yet undeveloped technology of "pico-engineering", where properties of devices require precise selection and placement of atoms, is a future chapter in Feynman's epic prediction "there's plenty of room at the bottom".[53)]

Acknowledgements

All the calculations were performed on the IMR Super Computer. The authors thank the staff of the SR8000 Supercomputer Facility, Institute for Materials Research, Tohoku University for their dedicated and enthusiastic support. MRP thanks the Center for Computational Materials Science for their warm hospitality and financial support. FC acknowledges support from the grant CNCSIS UEFISCU "Idei" 174/2007. MRP is a visiting scholar in the group of W. A. Lester at the Kenneth Pitzer Theory Centre, Chemistry Department, University of California-Berkeley.

REFERENCES

1) E. Clar: *Polycyclic hydrocarbons*, Vol. 1 and 2 (Academic Press, London, 1964).
2) E. Clar: *The Aromatic Sextet*, (Wiley, New York, 1972).
3) A. K. Geim and A. H. MacDonald: Physics Today **60** (2007) 35–41.
4) K. S. Novoselov, D. Jiang, F. Schedlin, V. V. Khotkevich, S. V. Morozov and A. K. Giem: PNAS (US) **102** (2005) 10451–10453.
5) C. Joachim, J. K. Gimzewski and A. Aviram: Nature **408** (2000) 541–548.
6) M. Y. Han, B. Ozyilmaz, Y. Zhang and P. Kim: Phys. Rev. Lett. **98** (2007) 206805-4.
7) C. D. Simpson, J. D. Brand, A. J. Berresheim, L. Przybilla, H. J. Raeder and K. Müllen: Chem. Eu. J. **8** (2002) 1424–1429.
8) A. C. Grimsdale and K. Müllen: Angew. Chem. Int. Ed. **44** (2005) 5592–5629.
9) K. N. Houk, P. S. Lee and M. Nendel: J. Org. Chem. **66** (2001) 5107.
10) M. Bendikov, H. M. Duong, K. Starkey, K. N. Houk, E. A. Carter and F. Wudl: J. Amer. Chem. Soc. Comm. **126** (2004) 7416-17.
11) E. Hückel: Z. Physik **70** (1931) 204.
12) E. Hückel: Z. Physik **72** (1931) 310.
13) E. Hückel: Z. Physik **76** (1932) 628.
14) D. P. Craig and N. L. Paddock: Nature **181** (1958) 1052–1053.
15) L. Salem: *The Molecular Orbital Theory of Conjugated Systems* (Benjamin, New York, 1966).
16) R. G. Parr: *Quantum Theory of Molecular-Electronic Structure* (Benjamin, New York, 1964).
17) I. Agranat: *Theoretical Aromatic Chemistry* in *Topics in Nonbenzenoid Aromatic Chemistry* ed. Nozoe, Breslow, Hafner, Ito and Murata, Vol. 1, Ch. 5, (Wiley, New York, 1973) pp. 139–178.
18) M. Randic: Chem. Rev. **103** (2002) 3449–3605.
19) P. v. R. Schleyer: Chem. Rev. **101** (2003) 1115–1116.
20) F. Sondheimer: Acc. Chem. Res. **5** (1972) 81–91.
21) G. Kresse and J. Hafner: Phys. Rev. **B47** (1993) 588–561.
22) G. Kresse and J. Hafner: Phys. Rev. **B49** (1994) 14251–14269.
23) G. Kresse and J. Furthmuller: Comput. Mater. Sci. **6** (1996) 15–50.
24) G. Kresse and J. Furthmuller: Phys. Rev. **B54** (1996) 11169–11186.
25) G. Kresse and J. Hafner: Phys. Rev. **B48** (1993) 13115–13118.
26) P. E. Blöchl: Phys. Rev. **B50** (1994) 17953–17979.
27) G. Kresse and J. Joubert: Phys. Rev. **B59** (1999) 1758–1775.
28) J. P. Perdew: *Electronic Structure of Solids 1991*, ed. P. Ziesche and H. Eschrig (Akademie-Verlag, Berlin, 1991).
29) J. P. Perdew, J. A. Chevary, S. H. Vosko, K. A. Jackson, M. R. Pederson, D. J. Singh and C. Fiolhais: Phys. Rev. **B46** (1992) 6671–6687.
30) Vaspview data viewer (http://vaspview.sourceforge.net); RASMOL structure viewer (http://www.umass.edu/microbio/rasmol/).
31) N. Zamstein, S. Kallush and B. Segev: J. Chem. Phys. **123** (2005) 074304-8.
32) F. Cimpoesu, M. R. Philpott, Y. Fujimura and Y. Kawazoe: *Aromaticity and anti-aromaticity in the triplet state of conjugated cyclic polyenes C_nH_n $(n = 4, 6, 8)$: Spin coupling and decoupling balance by DFT*. Unpublished results 2008.
33) S. Kivelson and O. L. Chapman: Phys. Rev. **B28** (1983) 7236–7243.
34) R. E. Peierls: *Quantum Theory of Solids* (Clarendon Press, Oxford, 1955).
35) W. T. Borden: *Diradicals*, ed. W. T. Borden (Wiley, New York, 1982).
36) M. C. dos Santos: Phys. Rev. **B74** (2000) 045426–045434.
37) C. Raghu, Y. A. Pati and S. Ramasesha: Phys. Rev. **B65** (2002) 155204-9.
38) C. Raghu, Y. A. Pati and S. Ramasesha: Phys. Rev. **B66** (2002) 035116-11.
39) J. Poater, J. M. Bofill, P. Alemany and M. Sola: J. Phys. Chem. A Letters **109** (2005) 10629–10632.
40) J. Hachmann, J. J. Dorando, M. Aviles and G. K.-L. Chan: J. Chem. Phys. **127** (2007) 134309-9.
41) S. E. Stein and R. L. Brown: J. Amer. Chem. Soc. **109** (1987) 3721–3729.
42) J. Fernandez-Rossier and J. J. Palacios: Phys. Rev. Letters **99** (2007) 177204-4.
43) W. L. Wang, S. Meng and E. Kaxiras: Nano Letters **8** (2008) 241–245.
44) B. Silvi and A. Savin: Nature **371** (1995) 683–686.
45) J. Poater, M. Duran, M. Sola and B. Silvi: Chem. Rev. **105** (2005) 3911–3947.
46) R. F. W. Bader: *Atoms in Molecules: A Quantum Theory* (Clarendon, Oxford, 1990).
47) D. P. Craig: Proc. Roy. Soc. (London) **A200** (1949) 401–409.
48) W. T. Simpson: J. Amer. Chem. Soc. **75** (1953) 597–603.
49) T. Hashimoto, H. Nakano and K. Hirao: J. Chem. Phys. **104** (1996) 6244–6258.
50) K. Hirao, H. Nakano, K. Nakayama and M. Dupuis: J. Chem. Phys. **105** (1996) 9227–9239.
51) H. J. Choi, D. Roundby, H. Sun, M. L. Cohen and S. G. Louie: Nature **418** (2002) 758–760.
52) M. R. Philpott and Y. Kawazoe: Chem. Phys. **348** (2008) 69–82. (http:dx.doi.org/10.1016/j.chemphys.2008.02.019).
53) R. P. Feynman: *Miniaturization*, ed. H. D. Gilbert (Reinhold, New York, 1960) Ch. 16, pp. 282–296.